Structural and electrochemical properties of high quality epitaxial titanium carbide thin films grown by pulsed laser deposition on MgO (111) and Al2O3 (001) substrates

Nicolas Ranger, Catalin-Daniel Constantinescu, Romain Lucas-Roper, Alexandre Boulle, Nicolas Glandut

Structural and electrochemical properties of high quality epitaxial titanium carbide thin films grown by pulsed laser deposition on MgO (111) and Al_2O_3 (001) substrates

Nicolas RANGER[1], **Catalin CONSTANTINESCU*[1,2], *Romain LUCAS-ROPER*[1], *Alexandre BOULLE*[1], *Nicolas GLANDUT*[1]

[1] *IRCER UMR 7315, CNRS / University of Limoges, 12 rue Atlantis, F-87000 Limoges, France*
[2] *LP3 UMR 7341, CNRS / University Aix-Marseille, 163 Avenue de Luminy, F-13009 Marseille, France*

Abstract

The electrochemical behaviour of titanium carbide (TiC_x, with $0.5 < x < 1$) thin films is presented and discussed with respect to their structural properties. Epitaxial (111)-oriented TiC films are grown onto (111)-cut MgO and (001)-cut Al_2O_3 substrates by using TiC targets with various stoichiometry. When using a TiC target, the films grown on Al_2O_3 substrates exhibit cyclic voltammograms significantly different from those grown on MgO. As a matter of fact, their electrochemical properties are strikingly similar to films with $TiC_{0.55}$ composition. It is demonstrated, by using high-resolution X-ray diffraction, that films grown on sapphire have a composition close to $TiC_{0.55}$, the driving force for carbon deficiency being the relaxation of the compressive interfacial strain at the Al_2O_3/TiC interface. On the contrary, the interfacial strain at the MgO/TiC interface is tensile which cannot be compensated by variations in the Ti/C ratio.

Keywords: *titanium carbide; laser ablation; thin films; electrochemistry; heteroepitaxy; stoichiometry.*
E-mail addresses: *nicolas.ranger@etu.unilim.fr, catalin.constantinescu@cnrs.fr, romain.lucas@unilim.fr, alexandre.boulle@cnrs.fr, nicolas.glandut@unilim.fr.*

1. Introduction

Titanium carbide (TiC_x) exists as a homogeneous phase over a wide range of stoichiometry, *i.e.*, a solid solution, with $0.5 < x < 1$. TiC is generally prepared in bulk from high-purity titanium dioxide blended with carbon black, between 1973 and 2373 K, with controlled carbon vacancy. TiC is a very hard, refractory material used in bulk, as thin films, or as nanoparticles [1-5], for manufacturing metal-working tools, high wear resistance, and lightweight parts and components. This non-oxide ceramic also finds usage as a catalysts support in hydrogenation-dehydrogenation processes, as well as for SO_2 decomposition and hydrotreating (hydrofining, hydrodesulfurization, hydrodearomatization) and reforming applications in the modern refinery to produce cleaner fuels, with excellent results especially when used in TiC (111) crystalline orientation [6-9].

The interest in developing TiC as thin films has recently further increased due to energy conversion applications breakthroughs, such as hydrogen storage and lithium intercalation, as electrodes in sensors, supercapacitors, and charge-storage devices, or in microwave absorption and electromagnetic protection [10-15]. However, the use of conventional methods to promote the growth of high purity carbide materials usually requires a substrate temperature in the range of 773 – 1273 K, while the technological requirements are to grow films at temperatures that do not surpass ~573 K.

Crystalline TiC thin films can be synthesized at any substrate temperature, including at room temperature, by using pulsed laser deposition (PLD) [1, 2]. This technique has already been widely used for its capability to evaporate and deposit refractory materials, *i.e.* iridium or INCONEL alloys.

Herein, we present and discuss on the electrochemical properties and the growth of TiC_x (x = 0.55 – 1.0) thin films with (111) crystallographic orientation, grown on (111)-cut MgO single-crystal substrates and on (001)-cut Al_2O_3 single-crystal. Their morphology and structure are investigated by atomic force microscopy (AFM), scanning electron microscopy (SEM), and high-resolution X-ray diffraction (HR-XRD). A comparison of the crystalline properties, the thickness and the morphology of the films is presented. Films are of high quality on all substrates tested and no delamination is observed. Subnanometric roughness and heteroepitaxial growth are observed in films grown both on MgO and Al_2O_3 substrates. The electrochemical properties of the films are rationalized with respect their crystallographic properties.

2. Experimental methods

2.1 Titanium carbide synthesis (bulk)

$TiC_{0.55}$ sample has been prepared by reactive hot pressing, directly from powder mixture of pure Ti and graphite, following the reaction: $Ti + 0.55C \rightarrow TiC_{0.55}$. Graphite powder (purity 99.5%, 325 mesh) was purchased from Cerac, USA, and titanium powder (purity 99.95%, <2 µm) from Neyco, France. Both have been used as received, without further purification. The powders, mixed together in pure acetone, were processed continuously by stirring for 24 h, and subsequently sintered in a furnace (1973 K and a pressure of 40 MPa) in a 15-mm graphite die, coated inside with boron nitride, BN. Pure argon atmosphere was used, to prevent oxidation. The temperature program was composed of a first segment from

ambient temperature to 1873 K at a rate of 0.25 K/s. Then, a second segment from 1873 to 1973 K at a rate of 0.016 K/s was used in order to avoid melting of unreacted titanium metal. Subsequently, the sintering temperature was reached at a rate of 0.25 K/s, and held for 3.5 h (*i.e.* 12 600 s). The 40 MPa pressure was applied at 1373 K, and released after the 3.5 h hold. To finish, the cooling from 1973 K to ambient was done at a rate of 0.16 K/s. The complete temperature program is shown in *Figure 1*. The stoichiometric compound ($TiC_{0.98\approx1}$) was also purchased from Cerac (purity 99.5%), used as provided, without any further purification, and sintered in the same manner as the $TiC_{0.55}$ bulk sample.

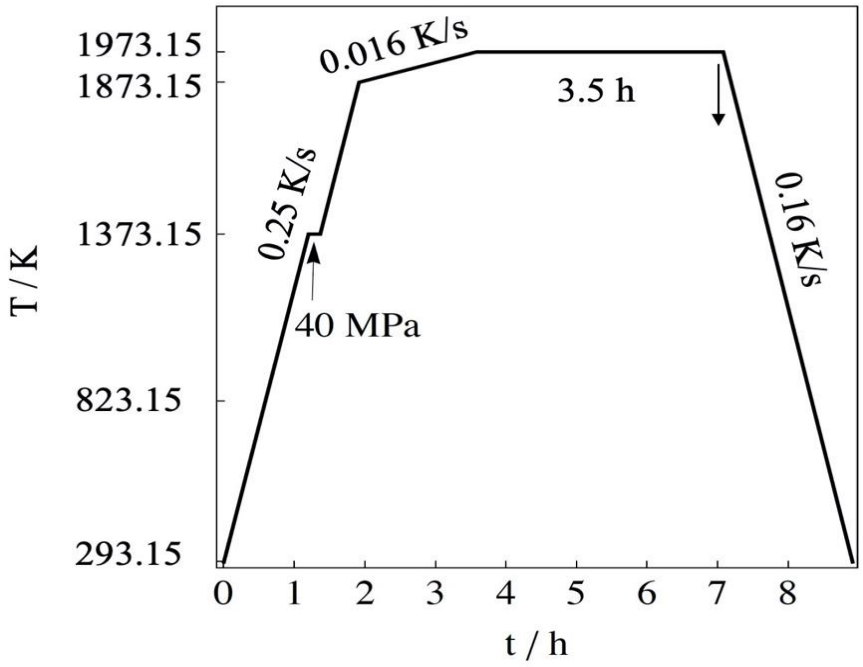

Figure 1: Temperature program used for the synthesis of the PLD targets, *i.e.* TiC and $TiC_{0.55}$.

2.2 Thin film growth (PLD)

As demonstrated below, the choice for these specific substrate types, *i.e.*, MgO(111) and Al_2O_3(001), allowed us to grow TiC_x films with the same (111) orientation, which facilitates the comparison between the two film/substrate systems. The substrates, thoroughly cleaned with isopropanol, ethanol and water, and finally dried in constant airflow, have been continuously monitored during the deposition by using a thermocouple. The deposition of TiC_x films was carried out in high vacuum (10^{-7} Pa), and at a temperature of 523 K, by using a KrF excimer laser (TuiLaser AG, model "Thin Film Star" / TFS 100-248nm-CT-T V2.0) operating at a

wavelength of 248 nm, 25 ns pulse duration, 20 Hz repetition rate (maximum), and at a fluence of 4,5 J/cm^2. The deposition time lasted for 30 minutes at a target-substrate distance of 4 cm.

2.3 Chemical, electrochemical, morphological, and structural investigations

Optical microscopy images have been taken to rapidly assess the quality of the films, with clear details as small as 1 µm, on a Kayence Optical Microscope. Scanning electron microscopy (SEM) has been used to assess information about the samples surface topography, composition, as well as about their thickness in a freshly broken/exposed cross-section. A field emission gun (FEG-SEM) setup from FEI (model Quanta FEG 450) equipped with a secondary electron detector (model SE R580) was used in order to avoid any bias that may be induced by the surface topography. Energy-dispersive X-ray spectroscopy (EDS) has been employed for the elemental analysis and chemical characterization of the samples. An EDS device from Oxford Instruments (model X-Max 150) equipped with a very large area (150 mm²) silicon drift detector (SDD) was used, installed in situ on the FEG-SEM setup. The AZtec analysis software from Oxford Instruments plc, UK was employed for analysis and data processing. Next, topographical observations were performed by using an atomic force microscope (AFM) on an Agilent AFM 5100 setup, with two-dimensional (2D) images and roughness parameters evaluated. High-resolution X-ray diffraction (HR-XRD) measurements were conducted on a Bruker D8 Discover diffractometer, equipped with Cu target (λ = 1.5406 Å), and a parabolic mirror associated with a two-reflection Ge monochromator. Diffracted X-rays are collected using a 1D (LynxEye) detector covering a 2° 2θ range with an angular resolution of 0.01°. Conventional θ-2θ scans and Φ-scans where performed to assess the film/substrate epitaxial relationships, whereas the level of strain was assessed by recording XRD reciprocal space maps (RSMs) from reflections with *hkl* indices containing both in-plane and out-of-plane components, by using the DxTools software [16]. Finally, electrochemical measurements have been carried out at room temperature, *i.e.*, 298 K, in a standard three electrode cell. An Autolab PGSTAT30 potentiostat was used, controlled by GPES software (EcoChemie, The Netherlands). The solution was a 0.1 M H_2SO_4 aqueous solution (Aldrich) and deionized ultrapure water (Millipore, Milli-Q, 18.2 MΩ.cm resistivity). It was deaerated by bubbling pure argon gas (Alphagaz 1, Air Liquide, France), prior to measurements, in order to remove dissolved oxygen, and argon gas was continuously blown onto the solution surface during the experiments. The contacts have been made directly with electrical clips and the samples were

dipped in the electrolyte. After each experiment, the submerged areas have been accurately measured by optical microscopy and subsequent image analysis (ImageJ software). The reference electrode was a K_2SO_4-saturated Hg/Hg_2SO_4 electrode. Potentials were recalculated *vs.* normal hydrogen electrode (NHE), *i.e.* 0.64 V was added. The counter electrode was a platinum disk (10 mm in diameter), and the working electrodes, consisted of the PLD-deposited films of titanium carbide on either MgO (111) or Al_2O_3(001).

3. Results and discussion

3.1 Optical, scanning and atomic force microscopy

Rapid optical microscopy observations revealed that no delamination effects are observed in our films. Top-view and cross-section SEM measurements reveal that the TiC films exhibit a smooth surface and a thickness of up to 200 nm on both substrates, and regardless of the targets stoichiometry, as presented in *Figure 2a* and *Figure 2b*, respectively.

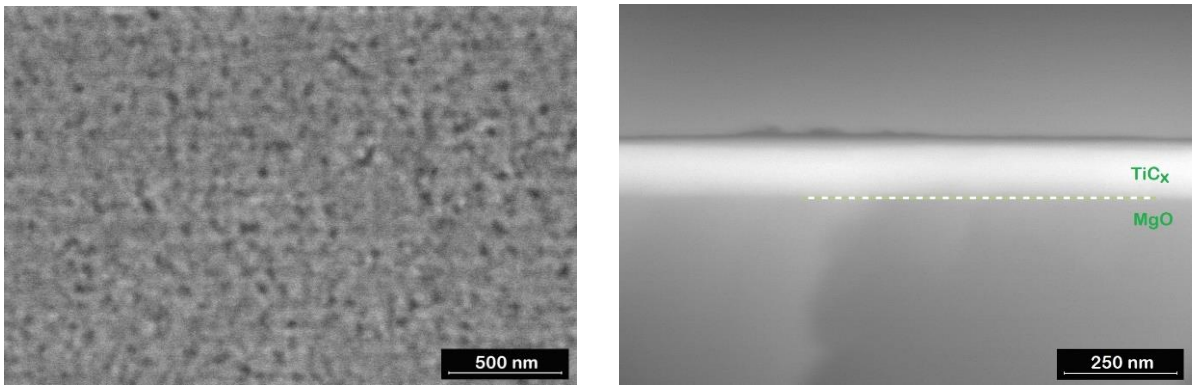

a.) *b.)*

Figure 2: Scanning electron microscope (SEM): top view (a) and cross-section (b) images of TiC on an MgO (111) substrates grown by PLD from a TiC target; film thickness: ~200 nm.

Additionally, topographic analyses have been carried out by AFM, as presented in *Figure 3*, revealing nanometric surface roughness for both type of substrates, expressed as the arithmetic average (Ra) of the roughness profile, *i.e.* Ra ≈ 0.258 nm for MgO substrates - *Figure 3a*, and Ra ≈ 0.138 nm for Al_2O_3(001) substrates - *Figure 3b*, as well as a certain structuring on the surface of these deposits. Such investigations are important to better assess the properties of the films. On one hand, the surface roughness may affect, induce and/or reveal internal defects in the thin film structure; on the other hand, the internal defects and/or stress of TiC thin films may affect the quality of their surface.

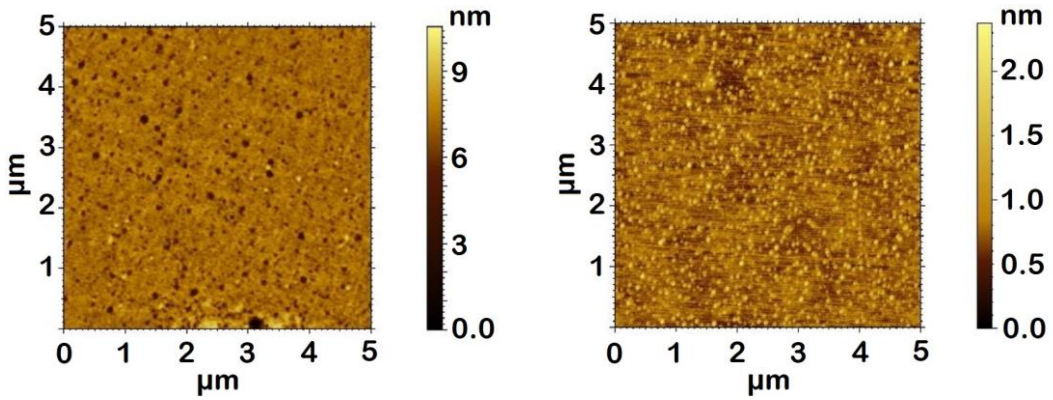

Figure 3: Atomic force microscope (AFM) image of TiC deposited by PLD from a TiC target on (a) MgO (111) substrates, and (b) on Al_2O_3(001) substrates.

3.2 Electrochemical investigations

Figure 4a shows the cyclic voltammogram obtained in 0.1 M H_2SO_4 aqueous solution for TiC film grown on MgO(111). A broad wave in oxidation can be observed, centred at 1.06 V *vs.* NHE, and with a peak current density of 750 µA cm^{-2}.

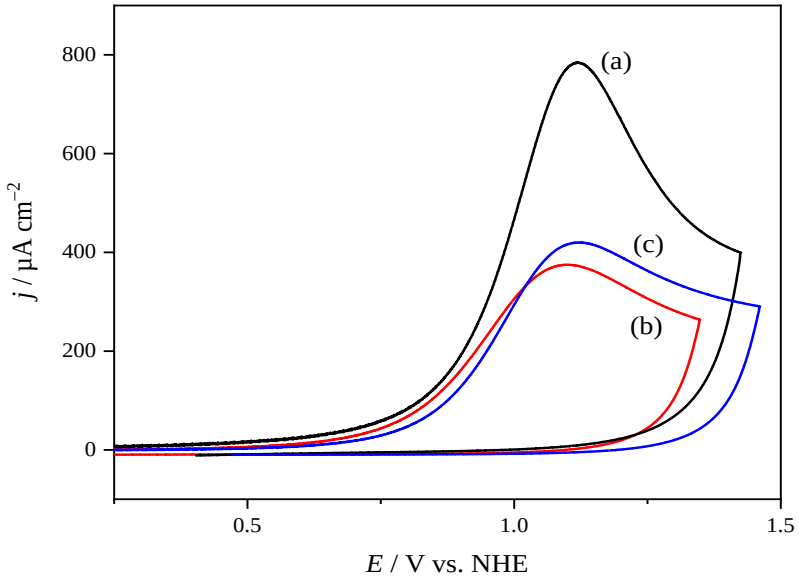

Figure 4: Cyclic voltammograms of TiC deposited by PLD, from a TiC target, for (a) MgO (111) substrate, and (b) sapphire Al_2O_3 (001) substrate. (c) From a $TiC_{0.55}$ target for both types of substrates. Aqueous solution: 0.1 M H_2SO_4. Scan rate: 100 mV s^{-1}. *T* = 298 K.

This corresponds to the electrochemical passivation of TiC by the formation of a hydrated titanium dioxide film, well-described now in the literature [17-20]. Carbon dioxide, which is the other thermodynamically stable compound [21], also evolves during this passivation and

the overall reaction for the entire potential range 0.8 ~ 1.3 V vs. NHE can be summarized as follows:

$$TiC + 5H_2O \rightarrow TiO_2.H_2O + CO_2 + 8H^+ + 8e^- \quad (1)$$

where n_1 = 8 electrons per TiC are involved. The charge integrated under the curve is ca. Q_1 = 2.4 mC cm^{-2}.

Figure 4b shows the same experiment as the previous one, in the case of the TiC / Al_2O_3 (001) system. It is worth emphasizing that the target used during growth is the same as the one used in the previous experiment, *i.e.* stoichiometric TiC. A broad wave in oxidation can still be observed, with the same simple shape, also centred at 1.06 V vs. NHE, but with a peak current density two times smaller. The charge under the curve is consequently smaller, ca. Q_2 = 1.75 mC cm^{-2}.

There are two possible causes for this result. The first is a composition change in the deposited carbide. This can be reasonably suggested because titanium carbide in its bulk form is well-known to possess a wide range of substoichiometry, *i.e.*, 0.5 < x < 1 in TiC_x [22, 23]. Let us assume that the deposited carbide on sapphire is $TiC_{0.5}$; the passivation reaction can then be rewritten:

$$TiC_{0.5} + 4H_2O \rightarrow TiO_2.H_2O + 0.5\ CO_2 + 6H^+ + 6e^- \quad (2)$$

where n_2 = 6 electrons are transferred. The charge being proportional to the number of electrons involved, we can therefore write $Q_1/Q_2 = n_1/n_2$. The ratio Q_1/Q_2 = 1.37, obtained from experiment, is very close to the ratio n_1/n_2 = 1.33, obtained from the theoretical electrochemical reactions. This is a clear indication that a drastic composition change for PLD-deposited TiC on Al_2O_3 (001) is highly probable, with a chemical formula close to $TiC_{0.5}$.

The second possible reason for $Q_2 < Q_1$ and a smaller current in the cyclic voltammograms could be the thickness of the TiO_2 passive layer formed. Indeed, the charge is also proportional to this thickness, and one could argue that oxidation does not occur to the same depth. To assess whether or not this mechanism takes place, other thin layers have been deposited by PLD, but with a bulk target made of $TiC_{0.55}$, and treated electrochemically. The result is displayed in *Figure 4c*. The shape and the orders of magnitude of the current and charge, are very similar to *Figure 4b*, and above all independent from the either substrate type, *i.e.* MgO (111) or Al_2O_3(001).

3.3 High-resolution energy-dispersive X-ray spectroscopy

In order to swiftly assess the carbon content of the materials (bulk and thin films), we used EDS. However, due to the high background counts in SEM-EDS, an artificial carbon peak is always visible and thus a value of more than 2% carbon is normally measured even in the raw substrates [24]. Although the SEM/EDS technique has historically been limited to relatively thick films when dealing with carbon-containing structures, and with more emphasis on film/surface morphology rather than compositional analysis, a reasonable difference in carbon content was found in the thin film samples as, corresponding to the TiC and $TiC_{0.5}$ structures (semi-quantitative analysis). Carbon signals are present on the EDS spectra of all samples, revealing carbon depletion for PLD-deposited TiC on Al_2O_3 (001). However, due to the high energies of incident electrons that are required to compensate for the low X-ray yield of carbon, appreciable penetration depths and low signal-to-noise ratio effects occur [25]. Thus, even with the use of modern surface-sensitive SEM and high-resolution EDS with low-noise electronics, the results must be corroborated by another high-resolution technique.

3.4 High-resolution X-ray diffraction analysis

To further support the scenario described above, we characterized the crystallographic structure of the TiC_x films, as grown on the MgO(111) and Al_2O_3(001) substrates. Conventional θ-2θ scans recorded from TiC/MgO and TiC/Al_2O_3 (not shown) reveal that only the *hhh* reflections of TiC and MgO and the 00*l* reflections of sapphire are present in the whole accessible angular range. This evidences that the (111) planes of TiC are parallel to (111) planes of MgO (in the case of TiC/MgO), and the (111) planes of TiC are parallel to the (001) planes of Al_2O_3 (in the case of TiC/Al_2O_3). This result is rather expected, with respect to previously published results, in similar systems [26, 27]

Φ-scans of the 113 reflection of TiC (in-plane orientations) are given in *Figure 5*. In the case of TiC/MgO, it can be straightforwardly noticed that the 113 peak position of TiC exactly correspond to the corresponding peak position of the substrate (black dotted line). The in-plane film/substrate orientation is therefore $[110]_{TiC}$ || $[110]_{MgO}$. This observation was also verified by HR-TEM on TiC films grown on MgO substrates (data not shown here). In the case of TiC/Al_2O_3 the situation is slightly complicated by the fact that the (111) plane of TiC exhibits a three-fold symmetry, whereas the (001) plane have a six-fold symmetry.

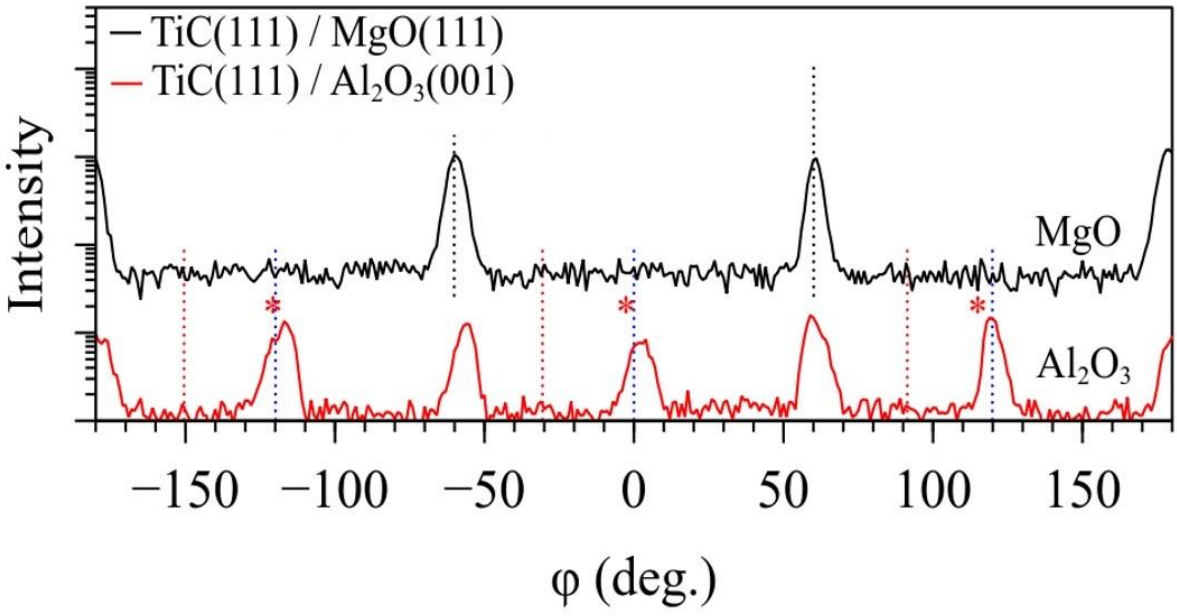

Figure 5: Φ-scans of the 113 reflection of TiC from the TiC/MgO system (upper, black line) and the TiC/Al_2O_3 system (lower, red line). The stars indicate the reflections originating from one epitaxial variant. The other reflections belong to the other variant.

There are therefore two equiprobable ways to grow TiC on Al_2O_3, which gives rise to two in-plane epitaxial variants. From the position of 018 peaks (red dotted lines), or the 119 peaks (blue dotted lines) of Al_2O_3, it can be concluded that one variant is such as $[110]_{TiC}$ || $[210]_{Al2O3}$ whereas the other is rotated by 60°, *i.e.* $[110]_{TiC}$ || $[120]_{Al2O3}$. This is also consistent with previously published results [28]. The fact that all peaks of the ϕ-scan have a similar intensity indicates that both variants are present in equal proportions.

Figure 6a shows a close-up of the θ-2θ scans in the vicinity of the 111 reflections of TiC. From this figure it can be observed that the 111-peak position of TiC differs depending on the underlying substrate, and that, in both cases, the peak position is smaller than the standard value of TiC (2θ = 35.907°, dotted line) [PDF card #00-32-1383] which indicates an elongation of the unit-cell in the direction normal to the surface. This elongation can be due either to a difference in the level of residual strains in the films and/or a different Ti/C molar ratio as compared to the reference material. In the case of epitaxial films, the respective effects of residual strains and composition can be disentangled by using XRD reciprocal space maps (RSMs) following a method previously used to analyse oxide and metallic films [29-31].

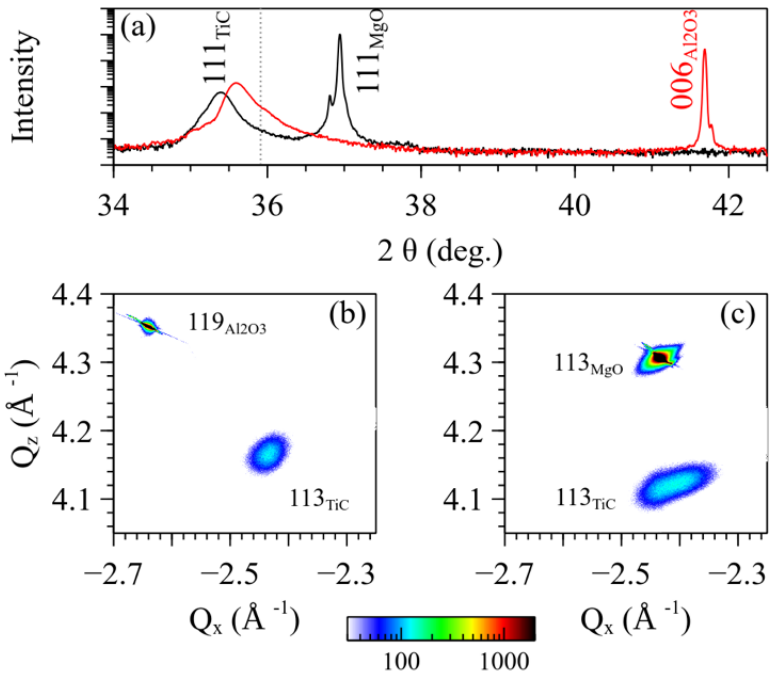

Figure 6: (***a***) θ-2θ scans in the vicinity of the 111 reflection of TiC.

Black line: TiC/MgO; red line: TiC/Al_2O_3; gray dotted line: standard TiC 111 peak position.

(***b***) and (***c***) RSMs recorded around the 113_{TiC} reflection in TiC/MgO and TiC/Al_2O_3, respectively.

The strain-free lattice parameter and the level of residual strain can be precisely derived by measuring the peak position (Q_x, Q_z) in *hhl* RSMs (*i.e.* reflections emanating from planes inclined with respect to the surface), for instance the 113 reflections. In this case, the x and z axes are parallel to the [110] and [111] directions, respectively, and the strain-free lattice parameter is obtained through:

$$d_x^{(bulk)} = \frac{d_z + d_x \times k \times \nu_2}{k \times (1 + \nu_2)}$$

where d_x and d_z are obtained from the RSM via $d_x = 2\pi / Q_x$ and $d_z = 2\pi / Q_z$, *k* is the theoretical d_{111}/d_{110} ratio in the TiC phase, and ν_2 the biaxial Poisson ratio, respectively. The former is equal to 0.565 and the latter is given by $(2C_{11} + 4C_{12} - 4C_{44}) / (C_{11} + 2C_{12} + 4C_{44})$, which equals 0.59368 using the C_{ij} values reported elsewhere [32].

Finally, the lattice strain is computed by using $e = (d_x - d_x^{(bulk)})/d_x^{(bulk)}$. 113 of RSMs of TiC are shown in *Figure 6(b,c)*. It should be emphasized that, in the case of C-deficient TiC materials, C vacancy might be non-randomly distributed, eventually leading to symmetry

changes [PDF card #04-017-1603], like for instance the Ti_2C phase. In the present work we verified that no such ordering occurs by carefully checking the lack of superstructure peaks characteristic of C-deficient phases in the θ-2θ scans (in particular around 2θ = 17.8° which correspond to the ½½½ superstructure peak of TiC_{1-x}). By using the above-mentioned approach, the in-plane strain of TiC/MgO is found e = –2.1%. This value is consistent with the value corresponding to the epitaxial (misfit) strain which, with the above mentioned in-plane epitaxial orientations, is -2.6%. The fact that both values are not equal indicates that part of the strain is relaxed during growth. This in-plane compressive strain is also consistent with out-of-plane elongation observed in *Figure 6a*. Surprisingly, the strain-free lattice parameter is found to be larger (4.3463 Å) than the value usually reported for TiC (4.3247 Å). The origin of this discrepancy is not yet understood, yet a couple of possible models might be envisaged in this context, to explain it:

1. Deviations from the 1:1 (Ti:C) stoichiometry cannot explain an increase in the lattice parameter [21]. Oxygen interdiffusion at the TiC/MgO cannot be straightforwardly excluded, even with the high vacuum during thin film depositions (at 10^{-7} Pa and even at 10^{-8} Pa), and may imaginably explain the dilatation of the unit cell [22]. Further work is due to validate or invalidate this hypothesis.

2. The derivation of the residual strain and the lattice parameter rely on the value of the elastic constants, C_{ij}, which are assumed to be known and equal to those of TiC. However, in the case of large deviations in the Ti/C molar ratio (*i.e.* the carbon deficiency / depletion), the C_{ij} values might also very likely deviate from their nominal value, hence casting some doubt regarding the exactness of the values derived previously. In such a situation, it is safer to consider those calculated values on a relative (rather than an absolute) scale.

Let us now consider the TiC/Al_2O_3 case. The epitaxial strain at the TiC/Al_2O_3 interface, using the orientations found above, is -9.7%. The value derived from the RSMs is -2%, which indicates a significant amount of strain relaxation, which is not unexpected. The strain-free lattice parameter is 4.3058 Å, which is also a very large deviation from the standard value, but in the opposite direction, *i.e.* we now observe a 0.5% contraction of the unit-cell. Bearing in mind the limitations evidenced in the TiC/MgO case, this value should not be considered as a perfectly precise measurement. However, since both films exhibit a similar level of residual strain (-2.1% and -2%), the difference in peak position in *Figure 6a* can only be accounted for by different bulk (strain-free) lattice parameter, *i.e.* $a_{MgO/Al2O3} < a_{MgO/TiC}$, which clearly points

to a loss of carbon in the material. For instance, the lattice parameter of $TiC_{0.62}$ (corrected for the unit-cell size doubling due to vacancy ordering) is 4.312 Å [PDF card #04-017-1603], which is only 0.14% different from our measurement. Additionally, according to [22] (Fig. 6 therein), a lattice parameter of 4.306 Å roughly corresponds to the $TiC_{0.55}$ composition, which corresponds to the value inferred from electrochemical measurements.

To conclude, a possible driving force for the loss of carbon is strain relaxation: during growth, the composition of the film varies to minimize the interfacial strain, a phenomenon sometime observed in oxide films exhibiting non-stoichiometry [29, 33].

4. Conclusion

Summarizing, in the present manuscript we report original research on the use of cyclic voltammetry corroborated with high-resolution X-ray diffraction in order to assess the carbon content of TiC thin films. For that, we have grown epitaxial TiC on MgO(111) and Al_2O_3(001) substrates by using pulsed laser deposition from TiC targets with various compositions. The films grown on sapphire substrates exhibit an electrochemical behaviour significantly different from those grown on MgO. Moreover, their cyclic voltammograms are strikingly similar to those of $TiC_{0.55}$ films although the deposition target is stoichiometric TiC. High-resolution X-ray diffraction measurements confirmed that films grown on sapphire are actually carbon deficient, with a composition of $TiC_{0.55}$, the driving force for the carbon deficiency being the relaxation of the compressive interfacial strain. On the contrary, the interfacial strain at the MgO/TiC interface is tensile which cannot be compensated by variations in the Ti/C ratio.

References

[1] P.M. Martin (editor): "*Handbook of Deposition Technologies for Films and Coatings: Science, Applications and Technology*" (3rd edition); Elsevier, New York (2010); ISBN: 978-0-8155-2031-3; https://www.sciencedirect.com/book/9780815520313/handbook-of-deposition-technologies-for-films-and-coatings

[2] N. Kaiser, "*Review of the fundamentals of thin-film growth*", Applied Optics 41, 3053 (2002); https://doi.org/10.1364/AO.41.003053

[3] R. Chang, L.J. Graham, "*Low-Temperature Elastic Properties of ZrC and TiC*", Journal of Applied Physics 37, 3778 (1966); https://doi.org/10.1063/1.1707923

[4] R. Kieffer, P. Schwarzkopf, F. Benesovsky, W. Leszynski, "*Hartstoffe und Hartmetalle*", Springer-Verlag, Vienna, (1953); ISBN 978-3-7091-3902-8 (in German); https://doi.org/10.1007/978-3-7091-3901-1

[5] K. Becker, F. Ebert, "*Die Kristallstrukturen einiger binaerer Carbide und Nitride*", Zeitschrift für Physik 31, 268 (1925) (in German); https://doi.org/10.1007/BF02980580

[6] Q. Zhang, L. Pastor-Pérez, S. Gu, T. Ramirez Reina, "*Transition Metal Carbides (TMCs) Catalysts for Gas Phase CO_2 Upgrading Reactions: A Comprehensive Overview*", Catalysts 10, 955 (2020); https://doi.org/10.3390/catal10090955

[7] S. Back, Y. Jung, "*TiC- and TiN-Supported Single-Atom Catalysts for Dramatic Improvements in CO_2 Electrochemical Reduction to CH_4*", ACS Energy Letters 2, 969–975 (2017); https://doi.org/10.1021/acsenergylett.7b00152

[8] J.A. Rodriguez, J. Evans, L. Feria, A.B. Vidal, P. Liu, K. Nakamura, F. Illas, "*CO_2 hydrogenation on Au/TiC, Cu/TiC, and Ni/TiC catalysts: Production of CO, methanol, and methane*", Journal of Catalysis 307, 162-169 (2013); https://doi.org/10.1016/j.jcat.2013.07.023

[9] J.A. Rodriguez, P.J. Ramírez, R.A. Gutierrez, "*Highly active Pt/MoC and Pt/TiC catalysts for the low-temperature water-gas shift reaction: Effects of the carbide metal/carbon ratio on the catalyst performance*", Catalysis Today 289, 47-52 (2017); https://doi.org/10.1016/j.cattod.2016.09.020

[10] A. Gringoz, N. Glandut, S. Valette, "*Electrochemical hydrogen storage in $TiC_{0.6}$, not in $TiC_{0.9}$*", Electrochemistry Communications 11, 2044 (2009); https://doi.org/10.1016/j.elecom.2009.08.049

[11] J. Nguyen, N. Glandut, C. Jaoul, P. Lefort, "*Electrochemical Hydrogen Insertion in Substoichiometric Titanium Carbide $TiC_{0.6}$: Influence of Carbon Vacancy Ordering*", Langmuir 29, 12036 (2013); https://doi.org/10.1021/la402043x

[12] J. Nguyen, N. Glandut, C. Jaoul, P. Lefort, "*Hydrogen insertion in substoichiometric titanium carbide*", International journal of hydrogen energy 40, 8562 (2015); https://doi.org/10.1016/j.ijhydene.2015.05.009

[13] J. Nguyen, "*Stockage électrochimique d'hydrogène dans le carbure de titane*", PhD Thesis (2013), University of Limoges (in French); http://www.theses.fr/2013LIMO4023.

[14] J. Bautista-Ruiz, J.C. Caicedo, A. Chaparro, "*Characterization of tungsten/titanium carbide coatings deposited by cathodic arc deposition for hydrogen evolution*", Rasayan

Journal of Chemistry 12, 1950 (2019); https://rasayanjournal.co.in/admin/php/upload/791_pdf.pdf

[15] V. Dev, "*Lithium intercalation studies in cubic titanium carbide thin films*", Applied Surface Science 449, 537 (2018); https://doi.org/10.1016/j.apsusc.2018.01.284

[16] A. Boulle, "*DxTools: processing large data files recorded with the Bruker D8 diffractometer*", Journal of Applied Crystallography 50, 967 (2017); https://doi.org/10.1107/S1600576717005192

[17] S. Saha, B.M. Rajbongshi, V. Ramani, A. Verma, "*Titanium carbide: An emerging electrocatalyst for fuel cell and electrolyser*", International Journal of Hydrogen Energy 46, 12801 (2021); https://doi.org/10.1016/j.ijhydene.2021.01.116

[18] A. Ignaszak, C. Song, W. Zhu, J. Zhang, A. Bauer, R. Baker, V. Neburchilov, S. Ye, S. Campbell, "*Titanium carbide and its core-shelled derivative TiC@TiO_2 as catalyst supports for proton exchange membrane fuel cells*", Electrochimica Acta 69, 397 (2012); https://doi.org/10.1016/j.electacta.2012.03.039

[19] B. Beverskog, J.O. Carlsson, A. Delblanc Bauer, C. V. Deshpandey, H. J. Doerr, R. F. Bunshah, B. P. O'Brien, "*Corrosion properties of TiC films prepared by activated reactive evaporation*", Surface and Coatings Technology 41, 221 (1990); https://doi.org/10.1016/0257-8972(90)90170-H

[20] H. E. Hintermann, A. C. Riddiford, R. D. Cowling, J. Malyszko, "*The anodic behaviour of titanium carbide in sulphuric acid solutions*", Electrodeposition and Surface Treatment 1, 59 (1972); https://doi.org/10.1016/0300-9416(72)90015-6

[21] M. Pourbaix, "*Atlas of Electrochemical Equilibria in Aqueous Solutions*", pp. 449-57, National Association of Corrosion Engineers, Houston, 1974; ISBN: 978-0-9155-6798-0; http://sunlight.caltech.edu/aic/pourbaix.pdf

[22] E. K. Storms, "*The Refractory Carbides*", Academic Press, New York, 1967; https://www.sciencedirect.com/bookseries/refractory-materials/vol/2/suppl/C; ISBN: 978-1-4832-3070-2

[23] A. I. Gusev, "*Phase equilibria, phases and compounds in the Ti–C system*", Russian Chemical Reviews 71, 439 (2002); https://doi.org/10.1070/RC2002v071n06ABEH000721

[24] J. Berlin, T. Salge, M. Falke, D. Goran, "*Recent Advances in EDS and EBSD Technology: Revolutionizing the Chemical Analysis of Chondritic Meteorites at the Micro and Nanometre*

scale", 42nd Lunar and Planetary Science Conference, 2723, (2011); https://www.lpi.usra.edu/meetings/lpsc2011/pdf/2723.pdf

[25] C. Puttichaem, G.P. Souza, K.C. Ruthe, K. Chainok, "*Characterization of Ultra-Thin Diamond-Like Carbon Films by SEM/EDX*", Coatings 11, 729 (2021); https://doi.org/10.3390/coatings11060729

[26] U. Jansson, H. Högberg, J.-P. Palmqvist, L. Norin, J. O. Malm, L. Hultman, J. Birch, "*Low temperature epitaxial growth of metal carbides using fullerenes*", Surface and Coatings Technology Volumes 142–144, 817 (2001); https://doi.org/10.1016/S0257-8972(01)01111-2

[27] J.-P. Palmquist; U. Jansson; T. Seppänen; P. O. Å. Persson; J. Birch; L. Hultman; P. Isberg, "*Magnetron sputtered epitaxial single-phase Ti_3SiC_2 thin films*", Appl. Phys. Lett. 81, 835 (2002); https://doi.org/10.1063/1.1494865

[28] P. Eklund, H. Högberg, L. Hultman, "*Epitaxial TiC/SiC multilayers*", Physica Status Solidi – Rapid Research Letters 1, 113 (2007); https://doi.org/10.1002/pssr.200701027

[29] V. Théry, A. Boulle, A. Crunteanu, J.C. Orlianges, "*Combined strain and composition-induced effects in the metal-insulator transition of epitaxial VO_2 films*", Applied Physics Letters 111, 251902 (2017); https://doi.org/10.1063/1.5010147

[30] L. Trupina, L. Nedelcu, M.G. Banciu, A. Crunteanu, L. Huitema, C. Constantinescu, A. Boulle, "*Texture and interface characterization of iridium thin films grown on MgO substrates with different orientations*", Journal of Material Science 55, 1753 (2020); https://doi.org/10.1007/s10853-019-04004-7

[31] H. Heinke, M.O. Möller, D. Hommel, G. Landwehr, "*Relaxation and mosaicity profiles in epitaxial layers studied by high resolution X-ray diffraction*", Journal of Crystal Growth 135, 41 (1994); https://doi.org/10.1016/0022-0248(94)90724-2

[32] D.Y. Dang, J.L. Fan, H.R. Gong, "*Thermodynamic and mechanical properties of TiC from ab initio calculation*", Journal Applied Physics 116, 033509 (2014); https://doi.org/10.1063/1.4890307

[33] F. Conchon, A. Boulle, R. Guinebretière, C. Girardot, S. Pignard, J. Kreisel, F. Weiss, E. Dooryhée, J.-L. Hodeau, "*Effect of tensile and compressive strains on the transport properties of $SmNiO_3$ layers epitaxially grown on (001) $SrTiO_3$ and $LaAlO_3$ substrates*", Applied Physics Letters 91, 192110 (2007); https://doi.org/10.1063/1.2800306